Artificial Intelligence Aided Automated Design for Reliability of Power Electronic Systems

Tomislav Dragičević, *Senior Member, IEEE*, Patrick Wheeler, *Senior Member, IEEE*, and Frede Blaabjerg, *Fellow, IEEE*

***Abstract*—This paper proposes a new methodology for automated design of power electronic systems realized through the use of artificial intelligence. Existing approaches do not consider the system's reliability as a performance metric or are limited to reliability evaluation for a certain fixed set of design parameters. The method proposed in this paper establishes a functional relationship between design parameters and reliability metrics, and uses them as the basis for optimal design. The first step in this new framework is to create a nonparametric surrogate model of the power converter that can quickly map the variables characterizing the operating conditions (e.g., ambient temperature and irradiation) and design parameters (e.g., switching frequency and dc link voltage) into variables characterizing the thermal stress of a converter (e.g., mean temperature and temperature variation of its devices). This step can be carried out by training a dedicated artificial neural network (ANN) either on experimental or simulation data. The resulting network is named as ANN_1 and can be deployed as an accurate surrogate converter model. This model can then be used to quickly map the yearly mission profile into a thermal stress profile of any selected device for a large set of design parameter values. The resulting data is then used to train ANN_2, which becomes an overall system representation that explicitly maps the design parameters into a yearly lifetime consumption. To verify the proposed methodology, ANN_2 is deployed in conjunction with the standard converter design tools on an exemplary grid-connected PV converter case study. This study showed how to find the optimal balance between the reliability and output filter size in the system with respect to several design constraints. This paper is also accompanied by a comprehensive dataset that was used for training the ANNs.**

***Index Terms*—Artificial intelligence, automated design for reliability (ADfR), power electronic systems.**

I. Introduction

THE use of power electronic converters has become omnipresent nowadays. They are the key enablers of technologies, such as renewable energy systems, electrical vehicles and their charging infrastructure, variable speed drives, as well as uninterruptible power supply systems and microgrids [1], [2]. Much like any other system, power converters are prone to failures. Such failures cause downtimes that often require costly maintenance procedures, especially if the power electronic system is located in the remote or offshore location. Moreover, such failures may also have catastrophic consequences in mission critical applications or significantly reduce the energy yield of renewable energy systems [3], [4].

Redundancy has historically been one of the most attractive approaches to provide the failure-tolerant capability to power electronic systems [5]. While being highly effective in this regard, redundant design will normally significantly increase the cost and size of the system, thus compromising its competitiveness in the market. Another scheme is to select the individual components in the converter (e.g., switching devices, inductors, and capacitors) with sufficient thermal and electrical stress margin, thus expecting their low failure rates and, consequently, high reliability of the overall system. However, with this approach, the quantitative reliability metrics of individual devices are not taken into account, and for this reason, it is also not possible to automatically design the system for prespecified lifetime.

To circumvent the drawbacks of aforementioned methods, the research in reliability of power electronic systems has recently experienced a paradigm shift toward the so-called design for reliability (DfR) approach [6], [7]. The key idea here is to take the reliability metrics explicitly into account during the design process. Since the most vulnerable part of power converters is semiconductor devices, the most attention in this research area has been dedicated toward studying their failure modes. To this end, it has been observed that the most common failure modes are associated with packaging, i.e., with die-attach solder fatigue and bond wire damage. Both of these modes are caused by junction temperature cycles and the mean junction temperature of the device during operation. Manufacturers of semiconductor devices have also carried out comprehensive temperature cycling tests and discovered functional relationships between the amplitude and mean value of the junction temperature, and the device lifetime consumption (LC) [8].

Therefore, the research focus in the DfR area has mostly been on investigating the thermal loading of power devices [9]–[11]. These investigations can be carried out either experimentally or using detailed simulations models, which have been shown to match excellently the experimental results [12], [13]. The main principle is to expose the power converter to a mission

Manuscript received July 5, 2018; revised September 15, 2018 and October 17, 2018; accepted November 26, 2018. Date of publication December 20, 2018; date of current version May 22, 2019. This work was supported in part by VILLUM FONDEN under the VILLUM Investigators Grant called REPEPS. Recommended for publication by Associate Editor B. Singh. *(Corresponding author: Tomislav Dragičević.)*

T. Dragičević and F. Blaabjerg are with the Department of Energy Technology, Aalborg University, Aalborg 9220, Denmark (e-mail: tdr@aau.dk; fbl@et.aau.dk).

P. Wheeler is with the Power Electronics, Machines and Control Group, The University of Nottingham, Nottingham NG7 2RD, U.K. (e-mail: pat.wheeler@nottingham.ac.uk).

Color versions of one or more of the figures in this paper are available online at http://ieeexplore.ieee.org.

Digital Object Identifier 10.1109/TPEL.2018.2883947

profile that represents its realistic operating condition and extract the corresponding thermal profile of one or more devices (i.e., the junction temperature data). The mission profile is usually characterized by an ambient temperature and current flowing through the power converter over a certain period of time [14]. The rainflow counting algorithm can then be deployed to count the number of junction temperature swings and to extract their amplitudes as well as mean values from the given thermal profile. Final step is to associate every cycle with its cumulative damage (e.g., using [8] or other device LC data from the relevant manufacturer), and calculate the overall LC over a period of time using the Miner's rule [9]. Assuming that all other components in the system are significantly more reliable, the LC of power devices is hence normally considered as the representation of the whole system's LC [15]–[18]. It is also possible to combine LCs of several components in the system to assess the system level LC [19].

Nevertheless, the LC estimation procedure in all the DfR approaches mentioned in the existing literature are made on power electronic systems whose design parameters are already fixed. This means that every time a designer would like to check how different design parameters affect the lifetime of power electronic system, he would need to perform the time-consuming simulations or experiments all over again. Moreover, with existing methods, it is not possible to specify a certain lifetime of the power electronic system as a design goal and then explicitly obtain the design parameters that guarantee the specified LC. In other words, there is no possibility to reverse the design process.

The aim of this paper is to bridge this research gap by building upon the principal DfR concepts and develop a fully automated design for reliability (ADfR) tool. The key enabling methodology for this development is artificial intelligence, and more particularly the artificial neural networks (ANNs). It is well known that ANNs are universal function approximators, i.e., they can approximate any given input/output data relationship with arbitrary precision [20]. Here, we take advantage of this capability for two different purposes. First, we use it to build a surrogate model of the power converter that is able to estimate the thermal stress of any device in the converter as a function of design parameters and the mission profile several orders of magnitude faster compared to running the detailed simulation model. Such a surrogate model, labeled as ANN_1, has similar functionality as a look-up table (LUT) reported in e.g., [18], but consumes significantly lower amount of memory, thus allowing to embed any design parameter as an input to the model. In addition, it has much better capability to generalize nonlinear input/output data relationship, thereby providing more precise estimates of the junction temperatures. The second purpose of ANN is to establish the functional relationship between design parameters and yearly LC in a network labeled ANN_2. Again, this process resembles the ones presented in [16]–[18], but here the LC evaluation is systematically repeated for a large number of design parameter variations to generate the training data for ANN_2 which, after training, gives an explicit functional relationship between design parameters and LC, thus providing a key basis for ADfR. ANN_2 can consequently be used either individually or in conjunction with other design tools, e.g., if it is desirable to balance the reliability of the system with other metrics such as cost, weight/volume, or others.

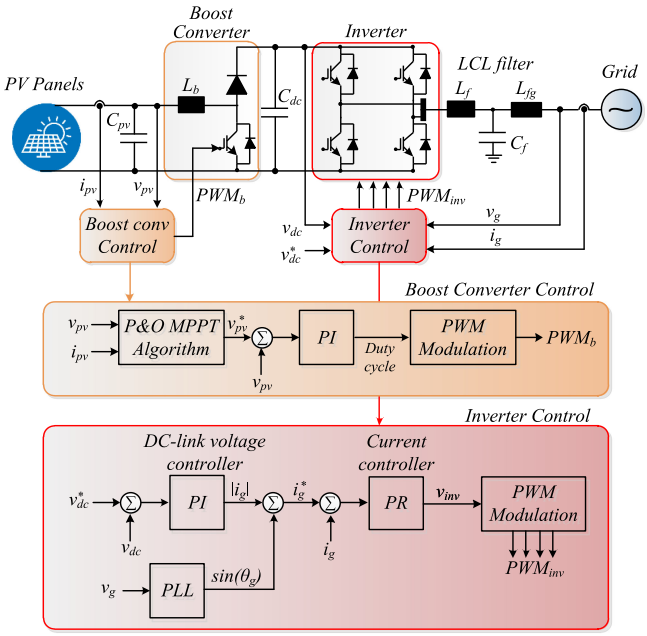

Fig. 1. System configuration and control structure of a two-stage single-phase grid-connected PV system. Here, PI is proportional-integral, PR is proportional-resonant, PLL is phase-locked loop, and PWM is pulsewidth modulator.

The rest of the paper is organized as follows. Section II describes the power electronic system under consideration, i.e., the single-phase grid-connected H-bridge PV inverter, although the proposed methodology is generic and thus applicable to any other converter topology. In Section III, the conventional system design and reliability evaluation methodologies are briefly revised, while Section IV provides the background about the ANNs. In Section V, the proposed design procedure is described step by step. The procedure is then verified in Section VI, where switching frequency and dc-link voltage reference of the grid-connected PV inverter that provide the optimal balance between the reliability and size of the system, are found via proposed approach. Finally, the conclusion of the paper is given in Section VII.

II. Description of the Case Study

A. System Description

The design methodology proposed in this paper is verified on a power electronic system case study that involves a two-stage grid-connected single-phase PV inverter with rated power of 10 kW, as shown in Fig. 1. The system comprises a dc–dc boost converter, which operates the maximum power point tracking algorithm and a full-bridge dc–ac converter that regulates the intermediate dc link voltage v_{dc} and grid side current using cascaded linear control loops. The correct angle for the current controller is provided by a phase-locked loop.

Table I indicates the design parameters of the system. These parameters have a strong influence on its performance, size/cost and reliability, and should therefore be carefully selected.

TABLE I
PARAMETERS OF THE TWO-STAGE SINGLE-PHASE PV SYSTEM (FIG. 1)

Fixed parameters	
PV inverter rated power	10 kW
Boost converter inductor	L_b = 1.8 mH
PV-side capacitor	C_{pv} = 1000 μF
Dc-link capacitor	C_{dc} = 1100 μF
Grid nominal frequency	$\omega_g = 2\pi \times 50 rad/s$
Grid nominal voltage (RMS)	230 V
Designable parameters	
Inverter LCL filter	L_f, C_f, L_{fg}
Inverter switching frequency	f_{sw}
Dc-link voltage reference	v^*_{dc}

In a case study analyzed in this paper, some of the listed parameters are considered to be fixed while others are designable. For instance, the switching frequency of the inverter f_{sw}, reference dc link voltage v^*_{dc}, and LCL filter parameters (L_f, C_f, L_{fg}) are chosen as designable parameters. By looking at the relationships between these parameters, it is intuitively clear that higher f_{sw} will yield a lower switching ripple, thus permitting the usage of a smaller filter. However, higher switching frequency will also result in higher switching losses, thereby causing larger junction temperatures of the power devices and shortening their lifetime.

While the aforementioned design tradeoff between the reliability and size of the system is well known, the existing research works fail to establish explicit relationships between these two metrics and to embed them as a part of the design process. More particularly, the works labeled under the *DfR* alias (e.g., [17], [18]) assume predetermined design and only provide lifetime prediction for a given design and mission profile. Therefore, it would be more appropriate to label the methods proposed in these works as reliability evaluation methods. On the other hand, the works that consider optimal design of power electronic systems (e.g., [21]–[24]) do not take into account the reliability of the system as a performance metric. The aim of this paper is to fill this knowledge gap by providing a holistic design methodology that simultaneously takes into account the performance, reliability, and size/cost of the system.

B. Mission Profile

Besides the design parameters, the mission profile in which the power converter is operated has a notable impact on the junction temperatures of power devices. Mission profile characterizes the operating conditions, such as the ambient temperature and the power processed by the converter. As shown in [18], mission profiles can vary significantly according to geographic location.

In this paper, a yearly mission profile recorded in Aalborg, Denmark has been used for the considered case study, as shown in Fig. 2. It can be seen from the figure that the profile involves yearly irradiation and ambient temperature data. Depending on the particular PV panel characteristics, which can be found in the manufacturer data-sheet, such data can easily be translated into the power processed by the inverter P_{in}, assuming that the maximum possible power is always extracted. P_{in} and T_a can then be used for obtaining the junction temperatures from the detailed simulation model, as detailed in Section III-B.

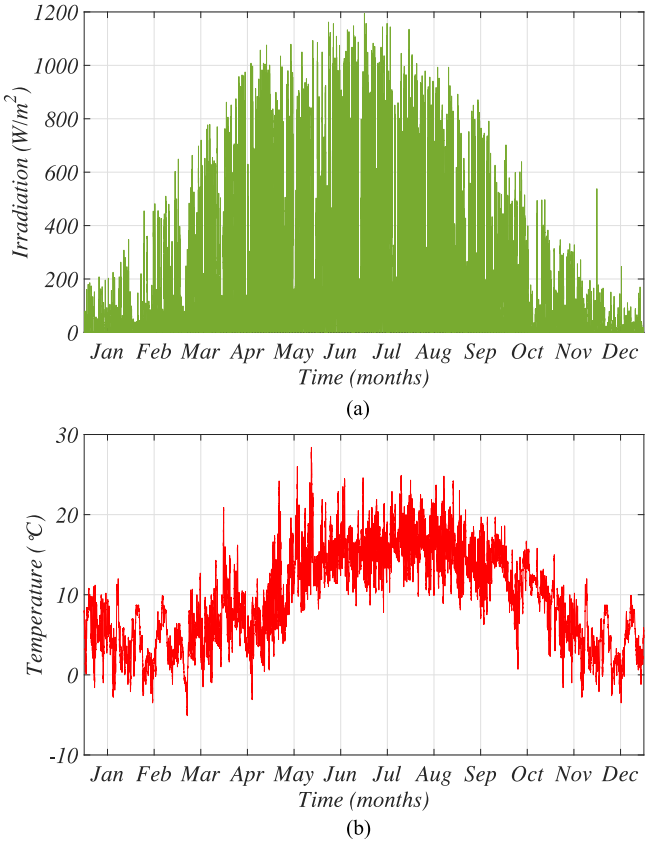

Fig. 2. Yearly mission profile from the PV installation site in Aalborg, Denmark with a sampling rate of 1 min/sample. (a) Solar irradiation. (b) Ambient temperature.

III. RELIABILITY OF THE POWER ELECTRONIC SYSTEM

In principle, the reliability of power electronic system can be improved in the following three ways [6]: First, by selecting a suitable topology of the converter, i.e., the one that either minimizes the number of components or that provides redundancy in case of failures, second, by choosing high-quality individual components in the system that are less likely to fail, and third, by reducing the stress level of the components [6].

A. Design Tradeoff

In this paper, it is assumed that the circuit topology of the converter is fixed and that the type of components most prone to failures, i.e., the switching devices, are preselected. To this end, the main design goal from a reliability point of view is to minimize the stress level on the switching devices. As mentioned before, lower f_{sw} leads to lower switching loss, which in turn induces lower temperature swings and hence leads to longer lifetime for the devices. However, lower f_{sw} also results in higher harmonic distortion and in a slower dynamic response of the converter, while it also requires bulkier and more expensive passive filters. Similarly, higher v_{dc} increases the switching losses and causes higher switching ripple [22], but the higher it

is, the more control bandwidth it provides [25]. In this respect, it is clear that f_{sw} and v_{dc} are two key design parameters that affect the reliability, performance, and size (cost) of the system. Therefore, these two parameters should be explicitly selected to yield the best balance between these metrics.

In order to provide a framework for truly optimal design, the well-known conventional design procedure (as in e.g., [21] and [22]) is here combined with the LC of the system, which can be considered as its reliability metric. The methodology for evaluating the LC of power devices is described in the following section.

B. Lifetime Evaluation Procedure

It is well known that the power devices are the most vulnerable components of power electronic converters. Depending on the mission profile (T_a and P_{in}) and design parameters (v_{dc}, f_{sw}, heat sink parameters, and others), these devices will experience junction temperature swings that cause their wear out. The temperature swings occur due to changing switching and conduction losses caused both by the varying loading (mission profile) and the sinusoidal shape of the inverter current. For a given operating condition, the thermal stress on the device can be characterized by the mean temperature value T_{jm}, the amplitude of oscillation ΔT_j, and the period of oscillation t_{ON}.

The concrete values of T_{jm}, ΔT_j, and t_{ON} can be extracted from the detailed simulation model of the converter and its associated thermal network. However, it is unfeasible to run the detailed simulation for the whole yearly mission profile period. For this reason, an approximate model of the converter that can quickly translate the mission profile and design parameters into junction temperatures, is commonly developed. The development of such model using artificial intelligence methodology is described in the following section.

For numerous types of devices, empirical models that quantify the effect of each cycle on the lifetime of the device have been constructed based on experimental data. An example of one such model is given in [8].

$$N_f = A \times (\Delta T_j)^{\alpha} \times (\text{ar})^{\beta_1 \Delta T_j + \beta_0} \times \left[\frac{C + (t_{\text{ON}})^{\gamma}}{C+1}\right] \times \exp\left(\frac{E_a}{k_b \times T_{\text{jm}}}\right) \times f_d \quad (1)$$

where N_f is the number of cycles that a device can tolerate before failure if stressed with a certain ΔT_j, T_{jm}, and t_{ON}. The other parameters required to evaluate (1) can be obtained experimentally. An exemplary set of parameters is taken from [8] and it is shown in Table II.

The inverse of N_f indicates the level of damage that a device sustains under certain stress conditions. In line with this, the total LC over a certain period can then be estimated using the Miner's rule as follows:

$$\text{LC} = \sum \frac{n_i}{N_{\text{fi}}} \quad (2)$$

where n_i is the number of cycles that result in incremental damage $1/N_{\text{fi}}$. Therefore, in order to find out the total LC that occurs over a certain time period, it is necessary to count the total number of temperature cycles and associate each cycle with a corresponding N_{fi}.

TABLE II
PARAMETERS OF THE LIFETIME MODEL OF AN IGBT MODULE

A	3.4368×10^{14}
α	-4.923
β_0	1.942
β_1	$-9.012x10^{-3}$
C	1.434
γ	-1.208
f_d	0.6204
ar	0.28
E_a	0.06606 eV
k_b	$8.6173324 \times 10^{-5} eV/K$

For a grid-connected PV system, two basic types of junction temperature cycles can be identified. The first type of cycles is caused by the mission profile and they are normally extracted from the yearly junction temperature data using the rain-flow counting algorithm. Such an algorithm extracts all the cycles and associates each one of them with a specific ΔT_j, T_{jm}, and t_{ON}, thus enabling the usage of (1). The second type is a repercussion of injecting the sinusoidal current at fundamental frequency into the grid. Therefore, this type has a fixed period t_{ON}, while given ΔT_j and T_{jm} can be extracted from the converter model and the rain-flow counting data, respectively. Therefore, the total LC can be calculated by adding the two contributions. It should also be noted that the parameters in (1) are usually not deterministic and can vary within certain ranges. If these effects are taken into account, the overall LC is normally evaluated using the Monte Carlo analysis and represented as the probability distribution function [26]. However, the consideration of the parameter variations in (1) is out of the scope of this paper, and will be considered in the future work.

IV. ANN-Based Modeling

A. Motivation for Using the ANNs

As explained in the previous section, it is essential to establish a simple model of the converter that would be able to translate the yearly mission profile data into a yearly junction temperature variation. The state-of-the-art approaches deal with this task by simulating the detailed model of the converter with associated thermal network for several selected combinations of P_{in} and T_a and extracting the corresponding ΔT_j and T_{jm}. These data are then fed to the LUT that serves as a surrogate model of the converter.

However, there are several fundamental limitations associated with this approach. First, LUTs are not suitable for high-dimensional data mapping, since they suffer from the inefficient use of memory space. This is particularly restricting if one would seek to construct a more complicated surrogate model of the power electronic system, where it would be required to map both the mission profile and design parameters to the junction temperatures. Second, LUTs are unable to learn general nonlinear relationships between the input data and output data, since they are based on linear interpolation. While the

second issue could be improved by using more data points, this would not be feasible in high-dimensional spaces due to limited memory. For these reasons, LUTs have been only used to map mission profile data (i.e., P_{in} and T_a) to junction temperatures, assuming that all other design parameters are fixed [18].

In order to come around this difficulty, in this paper, we propose the usage of a forward ANN to serve as a more fast, accurate, and flexible surrogate model of the converter. It has been shown in [20] that forward ANN is a universal function approximator, i.e., that the parameters in its structure can be adjusted in such a way to approximate any nonlinear input/output data relationship with arbitrary precision. For this reason, ANN has better generalization capability than LUT, and can thus better approximate the responses to input samples that are outside the training dataset. Another advantage of ANN is that the number of training parameters (i.e., weights and bias terms) can generally be several orders of magnitude lower than the number of data points. For this reason, ANN has much lower memory requirements than LUT. In particular, the evaluation of the ANN used in this paper was found to be around four orders of magnitudes faster than the LUT. Finally, ANN is based on a nonparametric regression model. In this case, designer does not need to know anything about the relationship between input and output data, because the ANN will learn them automatically during the training process. This is particularly useful in multidimensional spaces where parametric nonlinear regression approaches are not suitable, since it is difficult to guess the structure of the function that best models input–output data relationships.

The following section provides a brief theoretical introduction to ANNs.

B. ANN Principle

Numerous types of ANNs have been proposed in the literature [27]. Particular network choice depends mostly on the nature of relationships between inputs and outputs in the data. When outputs depend on historical values of the inputs and outputs, recurrent neural networks are the most suitable. In the case study of this paper, the relationship between design parameters and mission profiles with the junction temperatures is static. For this reason, forward ANN has been selected for the case study here. Forward ANNs are the most commonly used deep-learning algorithms and have been applied already to various electrical engineering problems, from predicting the voltage distortion in electrical distribution networks [28], to designing the microwave filters [29], [30].

A forward ANN comprises an input layer, one or more hidden layers, and an output layer. Each of these layers comprises a number of neurons that process the information coming from neurons in the layer below. To calculate the output of a certain neuron γ_i^l in layer l, the outputs of all the neurons z_j^{l-1} ($j = [1..N_{l-1}]$) in the layer below $l-1$ are multiplied with given weights ω_{ij}^l and the bias term b_i^l is then added. The result is processed through an activation function σ that usually takes the form of a sigmoid function, i.e., $\sigma(\gamma) = 1/(1+e^{-\gamma})$, to generate the output z_i^l. This output then becomes one of the inputs for the layer above, $l+1$, and the same procedure is repeated to calculate the output of other neurons in layer l.

In the input layer, z_i^1 takes the form of inputs. On the other hand, the output layer typically uses the linear activation function to allow any numerical value, as opposed to being limited to [0,1] range as the sigmoid function. To sum up, the complete signal flow of the ANN can be described as follows:

(1) Layer 1 (input):

$$z_i^1 = x_i \quad i = 1, .., N_1 \tag{3}$$

where x_i are the inputs.

(2) Layers $l = 2, .., L-1$ (hidden):

$$z_i^l = \sigma\left(\sum_{j=1}^{N_{l-1}} w_{ij}^l z_j^{l-1} + b_i^l\right) \quad i = 1, .., N_l. \tag{4}$$

(3) Layer L (output):

$$y_i = w_i^L z_i^L \quad i = 1, .., N_L \tag{5}$$

where y_i are the outputs.

It has been shown in [20] that forward ANN is an universal function approximator, i.e., that the weights and bias terms in its structure can be adjusted so as to approximate any input/output data relationships with arbitrary precision. These parameters are adjusted during the training process, normally using the back-propagation algorithm. This algorithm takes advantage of the continuous differentiability of the ANN to find out the direction in which the w_{ij}^l and b_i^l parameters should be adjusted in each training iteration to reduce the error between the measured output data and prediction made by the ANN from previous iterations [31]. Back-propagation is a well-known algorithm that is available in standard softwares like MATLAB.

It is important to notice that, before starting the training process, the structure of the network should be defined (i.e., the number of layers and the number of neurons in each layer). To this end, if too few neurons are used, the strong nonlinear relationships may not be captured. On the other hand, over-fitting may occur in ANNs with too many neurons. However, up until now, an analytic method for selection for proper number of neurons has not been established. Therefore, they are usually selected using trial-and-error and this approach is also used in this paper.

Next section presents the development of two ANNs that are used in the proposed optimal design procedure, which is detailed in Section V.

C. Deployment of ANNs for Fast and Flexible LC Evaluation of the PV Inverter

This section elaborates the development of two dedicated ANNs, one that serves as a surrogate model of the converter and one that translates the design parameters into a yearly LC.

1) ANN1: Surrogate Model of the PV Inverter: The purpose of this network is to map the operating conditions and design parameters into the junction temperatures and is labeled as ANN_1. The data required to train this network is collected

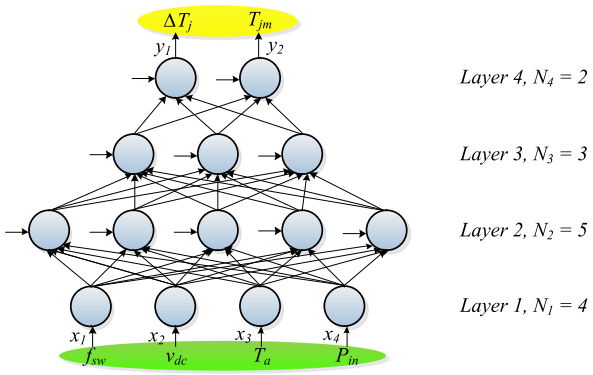

Fig. 3. Structure of the ANN_1. For simplicity, weights and bias terms are omitted from the figure. The inputs to the ANN_1 are highlighted with green color, while the outputs with yellow.

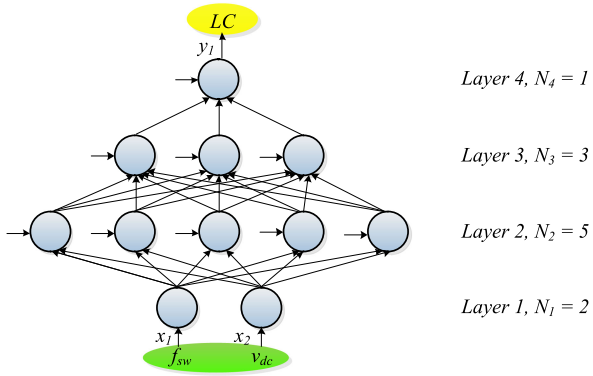

Fig. 4. Structure of the ANN_2. For simplicity, weights and bias terms are omitted from the figure. The inputs to the ANN_2 are highlighted with green color, while the outputs with yellow.

by running a detailed simulation model of the converter numerous times to cover some specific range of input parameter variations. After each simulation, corresponding $T_{jm,i,\text{data}}$ and $\Delta T_{j,i,\text{data}}$ are extracted.

Concerning the structure of the network, it has been empirically chosen to comprise an input layer, two hidden layers, and an output layer, and it is shown in Fig. 3. Therefore, there are 4 layers ($L = 4$) in total. The number of neurons in the input layer is 4 ($N_1 = 4$) since there are two design parameters v^*_{dc} and f_{sw} and two mission profile parameters, P_{in} and T_a. The number of layers in the two hidden layers are 5 and 3, respectively ($N_2 = 5$, $N_3 = 3$). Finally, the output layer comprises 2 neurons ($N_4 = 2$) because it is of interest to find out two values that characterize the junction temperature, i.e., its mean value T_{jm} and the amplitude of oscillation at fundamental frequency ΔT_j.

After specifying the datasets and structure of the network, ANN_1 was trained using the *train* command, which is a part of MATLAB's Deep Learning Toolbox. Trained ANN_1 can now be used to translate the tunable design parameters and the mission profiles given in Fig. 2 into a junction temperature of the inverter's devices for any given combination of design parameters v^*_{dc} and f_{sw}. Next, ANN_1 is put to use in order to create ANN_2, as detailed below.

2) ANN2: Mapping of Design Parameters to Lifetime of the Inverter: Besides ANN_1, another network labeled as ANN_2 is trained. This network serves as the overall representation of the system that maps the LC for a given yearly mission profile and design parameters. The data required to train this network is collected by running the cycle counting and performing the Miner's rule on a yearly junction temperature data (obtained by evaluating ANN_1 on a yearly mission profile data) for numerous combinations of design parameters f_{sw} and v^*_{dc}, as shown in Fig. 5. Therefore, ANN_1 is automatically embedded in ANN_2. Once the network is trained, instead of running the rainflow counting algorithm every time when the LC estimate is needed, the LC can simply be obtained by evaluating ANN_2.

The structure of this particular network is shown in Fig. 4. It was empirically selected to have an input layer, two hidden layers, and an output layer. The number of neurons in the input layer are 2 ($N_1 = 2$) since there are two design parameters v^*_{dc} and f_{sw}. The number of layers in the two hidden layers are 5 and 3, respectively ($N_2 = 5$, $N_3 = 3$). Finally, the output layer comprises 1 neuron ($N_4 = 1$) because our design interest is in one performance indicators, i.e., the converter yearly LC for a certain mission profile. After specifying the datasets and structure of the network, ANN_2 was again trained using the *train* command. Trained ANN_2 can now be deployed as a basis for the optimal design and combined with other designed methodologies, as described in the following section that provides the overall framework of the proposed design approach.

V. Proposed Automated Design Approach

The complete workflow of the proposed design approach is shown in Fig. 5. It can be seen that the procedure is split into a training phase that comprises four steps and an optimization stage with a single step. The training phase steps have been described in detail in the previous section and are only graphically summarized in Fig. 5. The ultimate result of this phase is trained ANN_2 that serves as the basis for optimal design, since it can explicitly map the design parameters to yearly LC.

Nevertheless, minimization of the LC often needs to be balanced with other metrics of the system. In this paper, the idea is to optimize the tradeoff between the LC and the system size, while respecting the performance metrics defined by relevant standards. To account for the power electronic system size in quantitative fashion, the standard methodology for the LCL filter design of grid-connected converters is adopted here (e.g., as suggested in [21] and [22]).

Similarly like with LC, the required LCL filter parameters are also dependent on the f_{sw} and v_{dc}. The first step is to select the inductance of the converter side inductor L_f, which is normally done in accordance with maximum permissible ripple in the converter current, as follows [22]:

$$L_f = \frac{v_{\text{dc}}}{6 f_{\text{sw}} \Delta I_{\text{Lmax}}}. \tag{6}$$

where ΔI_{Lmax} is usually selected to be 10% of the rated converter current. The filter capacitor C_f is then selected to limit the reactive power consumption of the filter. Usually, its value is

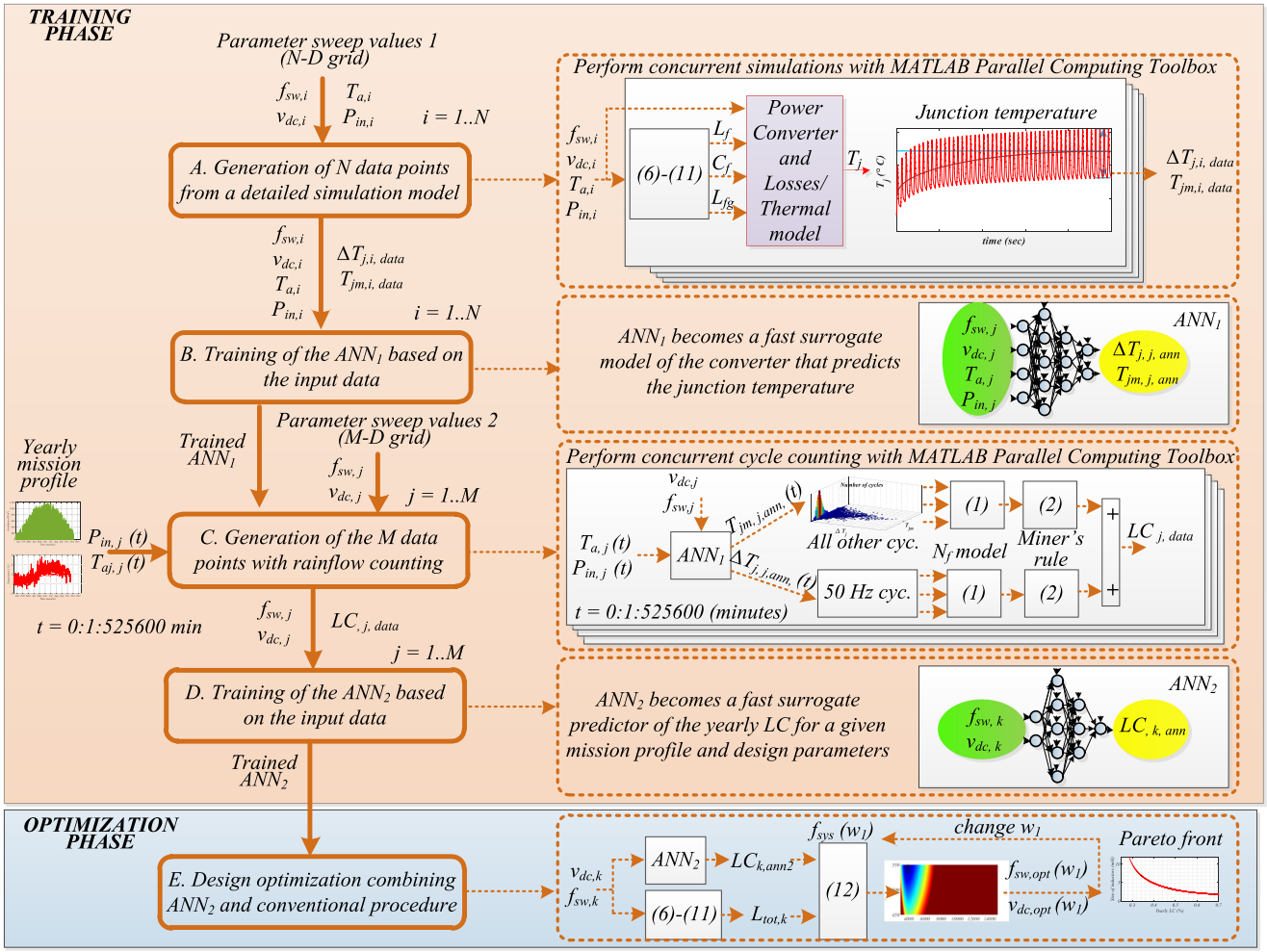

Fig. 5. Flow diagram of the proposed artificial intelligence based design optimization of the power electronic system.

limited to 5% of the base capacitance value, as follows:

$$C_f \leq 0.05 \cdot \frac{P_n}{\omega_g E_n^2}. \tag{7}$$

where P_n is the rated power of the converter, ω_g is the grid angular frequency, while E_n is the grid voltage amplitude. The attenuation of the harmonics from the converter side current depends also on the grid side inductor L_{fg}, as follows:

$$\frac{i_g}{i_c} = k_a = \frac{1}{1 + r(1 - L_f C_f \omega_{\text{sw}}^2)}. \tag{8}$$

where k_a is a required attenuation.

The (8) then provides the basis for the selection of L_{fg}

$$L_{\text{fg}} = \frac{\text{sqrt}(1/k_a^2) + 1}{C_f \omega_{\text{sw}}}. \tag{9}$$

It can be seen from (9) that the higher the C_f, the lower L_g is needed to achieve the same level of attenuation. Therefore, it is of interest to set the C_f at the upper limit in order to reduce the size of the L_g, which has a more dominant influence on the size of the system. It is also proposed in some references to initially select C_f at a value lower than maximum in order to allow sufficient headroom for iterative re-engineering the design if the resonance frequency of the filter does not meet the following mandatory requirement [21]:

$$10_{\text{fg}} < f_{\text{res}} = \frac{1}{2\pi}\sqrt{\frac{L_f + L_{\text{fg}} + L_g}{L_f\,(L_{\text{fg}} + L_g)\,C_f}} < 0.5 f_{\text{sw}}. \tag{10}$$

Finally, the resonant frequency is taken into account to derive the value for the damping resistor that is connected in series with the capacitor, as follows:

$$R_f = \frac{1}{6\pi f_{\text{ref}} C_f}. \tag{11}$$

To sum up, the standard LCL filter design methods take fixed f_{sw} and v_{dc} as inputs and provide the L_f, C_f and L_{fg} as outputs using the set of (6)–(10). It should also be noted that (6)–(10) can be used when generating the data for training ANN_1, as indicated in Fig. 5. Considering that there is not much freedom in designing C_f, it is proposed here to use the total size of inductors ($L_{\text{tot}} = L_f + L_{\text{fg}}$) alongside with the yearly LC (predicted by ANN_2) to formulate the overall fitness function, as follows:

$$f_{\text{sys}}(w_1) = \text{LC}_{\text{ann}}^2 + w_1 \cdot (L_{\text{tot}})^2. \tag{12}$$

where w_1 is the parameter that is used to balance the importance of the two terms. By using different values of w_1, a Pareto front that characterizes the relationships between the reliability and size of the system can be constructed.

The case-study analysis in the next chapter is carried out using the fitness function (12). However, it is important to notice that this particular fitness function is only exemplary and any other one can be easily adopted within the framework of proposed design methodology. For example, detailed calculation of total volume and power losses of the LCL filter has been carried out in [23] using comprehensive models of inductive power components. Consequently, a Pareto front indicating a tradeoff between volume and power loss of the filter has been derived. On the other hand, the LCL grid filter of a multimegawatt medium-voltage neutral-point-clamped converter for a wind turbine is designed using the selective harmonic elimination PWM in [24] to improve the converter efficiency. Design considerations concerning filter volume and efficiency could easily be embedded with the design process proposed in this paper by expanding the fitness function (12). Similarly, effect of alternative modulation schemes on converter efficiency could easily be considered by embedding any type of modulator in the simulation model from which the data is extracted. Consequently, the converter power loss could then be embedded in the fitness function (12) as well. Nevertheless, since research on advanced modulation schemes and detailed modeling of inductive components is out of the scope of this paper, these design considerations have not been considered in the case study carried out in the following section.

VI. Case Study

In order to verify the proposed design methodology, a case study for a PV system located in Denmark has been carried out. As already shown in Section II-B, irradiance and temperature data sampled minute by minute was available from a location in Aalborg/Denmark.

A. Data Extraction, Normalization, and Training

First and most computationally demanding step in the proposed method is to extract the data required to train ANN_1. A detailed simulation model of the grid connected inverter with associated heat sink and thermal networks was used for this purpose. The model was simulated for 3 s in order to ensure that the mean junction temperature converges to a steady-state value. Such simulation took around 2 min in real time.

In this paper, the design and mission profile parameters were swept using five values for each parameter except for the dc link voltage, where three values have been used (since the temperatures have been observed to rise linearly with the increasing dc link voltage). The main reason why this number of data points was enough to represent the power electronic system at hand is a monotonically increasing nature of underlying functional relationships between input and output data. For instance, if the converter processes higher amount of power, T_{jm} and ΔT_j will both be higher. Similarly, higher ambient temperature, higher switching frequency and higher dc link voltage will also cause increased temperatures of devices. Because of the monotonically increasing nature, the strong nonlinearity in these relationships is avoided and it turned out that it is possible to represent accurately the system only with limited number of data points. In this paper, the following parameter sweep values were used:

$$\begin{aligned} P_{\text{in}} &= [1000, 3000, 5000, 7000, 10\,000]\,\text{W} \\ V_{\text{dc}} &= [450, 500, 550]\,\text{V} \\ f_{\text{sw}} &= [3000, 5000, 7000, 10\,000, 15\,000]\,\text{Hz} \\ T_a &= [-10, 0, 15, 25, 35]\,^{\circ}\text{C}. \end{aligned} \tag{13}$$

Overall number of data points was thus 375 and the same number of simulations needed to be carried out to extract T_{jm} and ΔT_j. All the results were obtained in approximately 1 h on a workstation with 24 parallel cores using MATLAB's Parallel Computing Toolbox. The overall dataset can also be accessed in MATLAB (please find $data375.mat$ in the Active Content/Multimedia, where variables $Tmean$ and $deltaT$ correspond to the mean temperature and amplitude of temperature swing, respectively).

This dataset was then randomly divided into three datasets, i.e., the training set (70% of data, corresponding to 263 data points), the validation set (15% of data, corresponding to 56 data points), and the testing set (15% of data, corresponding to 56 data points). It should be noted that the precision of ANN turned out to be highly robust to data division ratios. Namely, empirical investigation has shown negligible differences in ANN precision if the training set was kept between 15% and 90% of overall data. Regular normalization technique was then deployed on the extracted data. To this end, the largest value of each data point was used as its norm and all other values of the same data type were then divided by the norm prior to the training. This procedure prevented the possibility of having different scales of input data, as all data points were in the [0, 1] range.

Consequently, ANN_1 was trained and passed the next stage, where it was used to generate data for yearly mission profile (see stage C., in Fig. 5). Here, the f_{sw} was swept from 3 to 15 kHz with a step of 1 kHz, whereas v_{dc}^{*} was swept from 450 to 550 V with a step of 10 V. Therefore, the total number of data points was 143. The whole data collection process was executed in less than 25 s, again by using MATLAB's Parallel Computing Toolbox. As mentioned before, 50 Hz junction temperature cycles were counted automatically while the other cycles were counted using a rainflow counting algorithm. As with ANN_1, this dataset was randomly divided into three datasets, i.e., the training set (70% of data, corresponding to 101 data points), the validation set (15% of data, corresponding to 21 data points), and the testing set (15% of data, corresponding to 21 data points). Data was also normalized. Finally, ANN_2 was trained on a given data and passed forward to the optimization phase.

B. Design Optimization

After the training phase was accomplished, trained ANN_2 was used in the optimization stage together with conventional design procedure, as indicated at the bottom of Fig. 5.

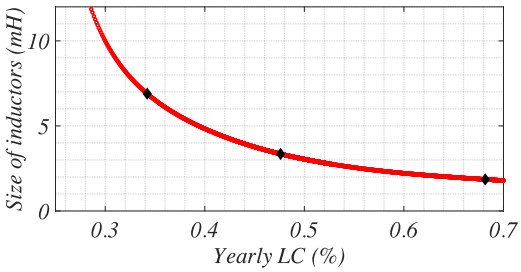

Fig. 6. Pareto front of optimal designs obtained by sweeping the parameter w_1 from (12) from 0 to 25. The three black diamonds correspond to $w_1 = 0.1$, $w_1 = 1$, and $w_1 = 10$, respectively (plots of corresponding fitness functions are shown in Figs. 7–9).

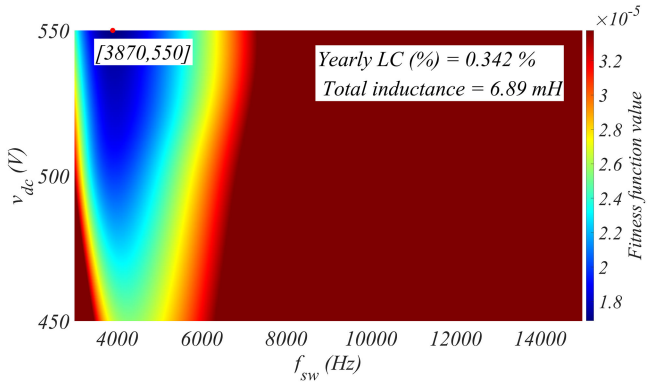

Fig. 7. Plot of the fitness function (12) for $w_1 = 0.1$. The optimum is achieved for $f_{\text{sw}} = 3870$ Hz and $v_{\text{dc}}^* = 550$ V, resulting in yearly LC of 0.342% and $L_{\text{tot}} = 6.89$ mH.

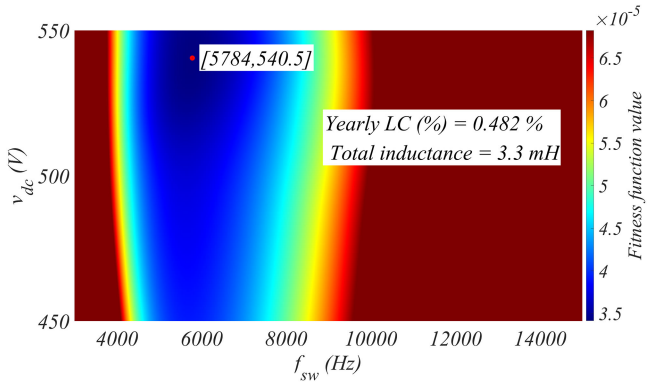

Fig. 8. Plot of the fitness function (12) for $w_1 = 1$. The optimum is achieved for $f_{\text{sw}} = 5784$ Hz and $v_{\text{dc}}^* = 540.5$ V, resulting in yearly LC of 0.482% and $L_{\text{tot}} = 3.3$ mH.

In particular, the minimum of the fitness function (12) was calculated for different parameter values of w_1, which was swept from 0 to 25. As an example, three arbitrary points corresponding to three different w_1 (for $w_1 = 0.1$, $w_1 = 1$, and $w_1 = 10$, respectively) have been selected from a given curve. The super-high-fidelity plots of associated fitness functions (together with optimal design parameters and corresponding total filter inductance, as well as LC) are given in Figs. 7–9, respectively. The respective minimums have been found using an exhaustive search algorithm, which is feasible for this case study, since the evaluation of ANN_2 is computationally extremely light (around

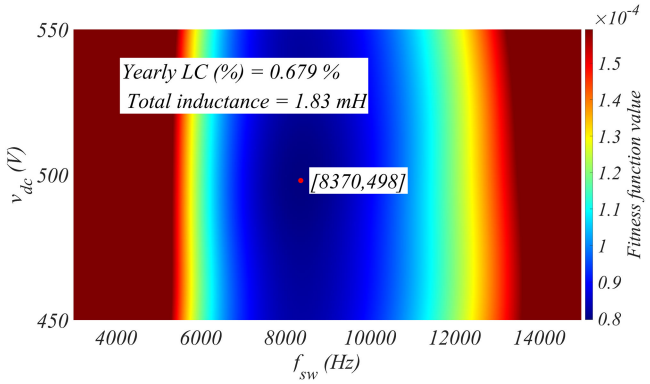

Fig. 9. Plot of the fitness function (12) for $w_1 = 10$. The optimum is achieved for $f_{\text{sw}} = 8370$ Hz and $v_{\text{dc}}^* = 498$ V, resulting in yearly LC of 0.679% and $L_{\text{tot}} = 1.83$ mH.

0.1 μs). For comparison, a commonly used LUT that comprises the same dataset turned out to be significantly more computationally intensive as it took approximately 800 μs to evaluate it. While this time can still be considered relatively short, it would quickly present a limitation when sweeping through the whole design space with high fidelity.

Fig. 6 shows the Pareto front that shows the yearly LC and the filter size corresponding to minimums of many fitness functions obtained by sweeping the parameter w_1 from 0 to 25. The obtained Pareto front clearly illustrates the tradeoff between the yearly LC and size of the system and provides the formal framework for optimal design. Considering fast evaluation of the fitness function (12), each of the four-megapixel plots shown in Figs. 7–9 were generated in less than 0.5 s. The optimal solution was then simply obtained by finding the lowest value in the given plot, which can be done in MATLAB almost instantaneously using the embedded min function.

It also needs to be noted that if more design parameters should be considered, the computational burden of the exhaustive search method might become too high. If this happens, there are several alternative ways to do the minimization. One possibility may be to evaluate fitness function sequentially, with higher and higher fidelity. Another option could be to apply advanced approaches, such as evolutionary optimization. This would not impose strict limitation on the number of design parameters, but would bring risk of getting stuck in local minimums.

VII. Conclusions and Future Work

In this paper, an artificial intelligence aided methodology for design optimization of power electronic systems has been proposed. The fundamental idea behind the method is to substitute the key two steps of the system's standard reliability evaluation procedure with dedicated ANNs that serve as fast and accurate approximations of these steps. As shown in Fig. 5, the first one, ANN_1, is trained to act as a surrogate model of the power electronic converter that can map the operating conditions and design parameters into junction temperature(s) of the converter's power devices. The other one, ANN_2, is then trained using both ANN_1 and any given mission profile (e.g.,

yearly) to serve as an overall system representation that maps the design parameters into a LC. Since ANN can be evaluated extremely fast (around 1 μs), numerous design parameter combinations can be tested almost instantaneously in order to shed light on their influence of design goals. Here, this capability was exploited in order to formally investigate the influence of two exemplary design parameters, i.e., f_{sw} and v_{dc}^{*} on the tradeoff between the filter size in the single-phase grid-connected PV system and the LC of the devices in the converter. With aid of proposed methodology, this tradeoff was represented with the Pareto curve that provides the precise design limitations of the system and allows one to analytically find the optimal f_{sw} and v_{dc}^{*} in accordance to desired position on the Pareto curve. This provides a clear improvement over the state of the methods that can only evaluate the LC for a fixed design and allows powerful design optimization capability. Possible interesting directions for the future work could be to look at more design parameters (e.g., heat sink parameters, modulation strategy, etc.). This would prolong the data extraction process, but the trained neural network could then be used for more comprehensive design optimization. Another research direction could be to embed more performance metrics, such as the volume and cost of the system. Finally, it would be interesting to investigate the proposed system design procedure on types of power electronic converters that exhibit unequal thermal stress distribution among their devices.

ACKNOWLEDGMENT

The authors would like to thank A. Sangwongwanich for his help in setting up the simulation model of the power electronic system as shown in Fig. 1.

REFERENCES

[1] F. Blaabjerg, Z. Chen, and S. Kjaer, "Power electronics as efficient interface in dispersed power generation systems," *IEEE Trans. Power Electron.*, vol. 19, no. 5, pp. 1184–1194, Sep. 2004.

[2] T. Dragicevic, X. Lu, J. C. Vasquez, and J. M. Guerrero, "DC microgrids—Part II: A review of power architectures, applications, and standardization issues," *IEEE Trans. Power Electron.*, vol. 31, no. 5, pp. 3528–3549, May 2016.

[3] A. Golnas, "PV system reliability: An operator's perspective," *IEEE J. Photovolt.*, vol. 3, no. 1, pp. 416–421, Jan. 2013.

[4] V. N. Ferreira, A. F. Cupertino, H. A. Pereira, A. V. Rocha, S. I. Seleme, and B. Cardoso, "Design and selection of high reliability converters for mission critical industrial applications: A rolling mill case study," *IEEE Trans. Ind. Appl.*, vol. 54, no. 5, pp. 4938–4947, Sep./Oct. 2018.

[5] J. C. Salmon, "Reliable 3-phase PWM boost rectifiers employing a stacked dual boost converter subtopology," *IEEE Trans. Ind. Appl.*, vol. 32, no. 3, pp. 542–551, May/Jun. 1996.

[6] R. Burgos, G. Chen, F. Wang, D. Boroyevich, W. G. Odendaal, and J. D. V. Wyk, "Reliability-Oriented design of three-phase power converters for aircraft applications," *IEEE Trans. Aerosp. Electron. Syst.*, vol. 48, no. 2, pp. 1249–1263, Apr. 2012.

[7] H. Wang, M. Liserre, and F. Blaabjerg, "Toward reliable power electronics: Challenges, design tools, and opportunities," *IEEE Ind. Electron. Mag.*, vol. 7, no. 2, pp. 17–26, Jun. 2013.

[8] U. Scheuermann, R. Schmidt, and P. Newman, "Power cycling testing with different load pulse durations," in *Proc. 7th IET Int. Conf. Power Electron. Mach. Drives*, Apr. 2014, pp. 1–6.

[9] H. Huang and P. A. Mawby, "A lifetime estimation technique for voltage source inverters," *IEEE Trans. Power Electron.*, vol. 28, no. 8, pp. 4113–4119, Aug. 2013.

[10] A. Anurag, Y. Yang, and F. Blaabjerg, "Thermal performance and reliability analysis of single-phase PV inverters with reactive power injection outside feed-in operating hours," *IEEE J. Emerg. Sel. Topics Power Electron.*, vol. 3, no. 4, pp. 870–880, Dec. 2015.

[11] M. Andresen, G. Buticchi, and M. Liserre, "Thermal stress analysis and MPPT optimization of photovoltaic systems," *IEEE Trans. Ind. Electron.*, vol. 63, no. 8, pp. 4889–4898, Aug. 2016.

[12] K. Ma, M. Liserre, F. Blaabjerg, and T. Kerekes, "Thermal loading and lifetime estimation for power device considering mission profiles in wind power converter," *IEEE Trans. Power Electron.*, vol. 30, no. 2, pp. 590–602, Feb. 2015.

[13] A. S. Bahman, K. Ma, P. Ghimire, F. Iannuzzo, and F. Blaabjerg, "A 3-D-lumped thermal network model for long-term load profiles analysis in high-power IGBT modules," *IEEE J. Emerg. Sel. Topics Power Electron.*, vol. 4, no. 3, pp. 1050–1063, Sep. 2016.

[14] S. E. D. Len-Aldaco, H. Calleja, F. Chan, and H. R. Jimnez-Grajales, "Effect of the mission profile on the reliability of a power converter aimed at photovoltaic applications—A case study," *IEEE Trans. Power Electron.*, vol. 28, no. 6, pp. 2998–3007, Jun. 2013.

[15] Y. Song and B. Wang, "Survey on reliability of power electronic systems," *IEEE Trans. Power Electron.*, vol. 28, no. 1, pp. 591–604, Jan. 2013.

[16] M. Musallam, C. Yin, C. Bailey, and M. Johnson, "Mission profile-based reliability design and real-time life consumption estimation in power electronics," *IEEE Trans. Power Electron.*, vol. 30, no. 5, pp. 2601–2613, May 2015.

[17] N. C. Sintamarean, F. Blaabjerg, H. Wang, F. Iannuzzo, and P. de Place Rimmen, "Reliability oriented design tool for the new generation of grid connected PV-inverters," *IEEE Trans. Power Electron.*, vol. 30, no. 5, pp. 2635–2644, May 2015.

[18] A. Sangwongwanich, Y. Yang, D. Sera, and F. Blaabjerg, "Lifetime evaluation of grid-connected PV inverters considering panel degradation rates and installation sites," *IEEE Trans. Power Electron.*, vol. 33, no. 2, pp. 1225–1236, Feb. 2018.

[19] D. Zhou, G. Zhang, and F. Blaabjerg, "Optimal selection of power converter in DFIG wind turbine with enhanced system-level reliability," *IEEE Trans. Ind. Appl.*, vol. 54, no. 4, pp. 3637–3644, Jul./Aug. 2018.

[20] K. Hornik, M. Stinchcombe, and H. White, "Multilayer feedforward networks are universal approximators," *Neural Netw.*, vol. 2, no. 5, pp. 359–366, 1989.

[21] M. Liserre, F. Blaabjerg, and S. Hansen, "Design and control of an LCL-filter-based three-phase active rectifier," *IEEE Trans. Ind. Appl.*, vol. 41, no. 5, pp. 1281–1291, Sep./Oct. 2005.

[22] A. Reznik, M. G. Simoes, A. Al-Durra, and S. M. Muyeen, "LCL filter design and performance analysis for grid-interconnected systems," *IEEE Trans. Ind. Appl.*, vol. 50, no. 2, pp. 1225–1232, Mar./Apr. 2014.

[23] J. Muhlethaler, M. Schweizer, R. Blattmann, J. W. Kolar, and A. Ecklebe, "Optimal design of LCL harmonic filters for three-phase PFC rectifiers," *IEEE Trans. Power Electron.*, vol. 28, no. 7, pp. 3114–3125, Jul. 2013.

[24] M. Zabaleta, E. Burguete, D. Madariaga, I. Zubimendi, M. Zubiaga, and I. Larrazabal, "LCL grid filter design of a multimegawatt medium-voltage converter for offshore wind turbine using SHEPWM modulation," *IEEE Trans Power Electron*, vol. 31, no. 3, pp. 1993–2001, Mar. 2016.

[25] D. G. Holmes, T. A. Lipo, B. P. McGrath, and W. Y. Kong, "Optimized design of stationary frame three phase ac current regulators," *IEEE Trans. Power Electron.*, vol. 24, no. 11, pp. 2417–2426, Nov. 2009.

[26] P. D. Reigosa, H. Wang, Y. Yang, and F. Blaabjerg, "Prediction of bond wire fatigue of IGBTs in a PV inverter under a long-term operation," *IEEE Trans. Power Electron.*, vol. 31, no. 10, pp. 7171–7182, Oct. 2016.

[27] J. Schmidhuber, "Deep learning in neural networks: An overview," *Neural Netw.*, vol. 61, pp. 85–117, 2015.

[28] B. Singh, V. Verma, and J. Solanki, "Neural network-based selective compensation of current quality problems in distribution system," *IEEE Trans. Ind. Electron.*, vol. 54, no. 1, pp. 53–60, Feb. 2007.

[29] Q.-J. Zhang, K. C. Gupta, and V. K. Devabhaktuni, "Artificial neural networks for RF and microwave design—From theory to practice," *IEEE Trans. Microw. Theory Techn.*, vol. 51, no. 4, pp. 1339–1350, Apr. 2003.

[30] H. Kabir, Y. Wang, M. Yu, and Q. J. Zhang, "Neural network inverse modeling and applications to microwave filter design," *IEEE Trans. Microw. Theory Techn.*, vol. 56, no. 4, pp. 867–879, Apr. 2008.

[31] D. E. Rumelhart, G. E. Hinton, and R. J. Williams, "Learning representations by back-propagating errors," *Nature*, vol. 323, pp. 533–536, Oct. 1986.

Tomislav Dragičević (S'09–M'13–SM'17) received the M.Sc. and the Industrial Ph.D. degrees in electrical engineering from the Faculty of Electrical Engineering, Zagreb, Croatia, in 2009 and 2013, respectively.

From 2013 until 2016, he was a Postdoctoral Research Associate with Aalborg University, Aalborg, Denmark. From March 2016, he has been an Associate Professor with Aalborg University, where he leads the Advanced Control Lab. He was a Guest Professor with Nottingham University, Nottingham, U.K., during Spring/Summer of 2018. His research interests include design and control of microgrids and application of advanced modeling and control concepts to power electronic systems. He has authored and coauthored more than 155 technical papers (more than 55 of them are published in international journals, mostly IEEE Transactions) in his domain of interest, 8 book chapters, and a book in the field. He has also edited a book on microgrids. He serves as an Associate Editor for IEEE TRANSACTIONS ON INDUSTRIAL ELECTRONICS, IEEE EMERGING AND SELECTED TOPIC IN POWER ELECTRONICS, and in the *Journal of Power Electronics*. He was the recipient of the Končar Prize for the Best Industrial Ph.D. thesis in Croatia and the Robert Mayer Energy Conservation award.

Patrick Wheeler (M'90–SM'04) received the B.Eng. (Hons.) degree, in 1990, and the Ph.D. degree in electrical engineering for his work on matrix converters both from the University of Bristol, Bristol, U.K. in 1994.

He was a Research Assistant with the Department of Electrical and Electronic Engineering, University of Nottingham, Nottingham, U.K., in 1993. In 1996, he became a Lecturer in the Power Electronics, Machines and Control Group with the University of Nottingham. Since January 2008, he has been a Full-time Professor with the same research group. He was the Head of the Department of Electrical and Electronic Engineering with the University of Nottingham, from 2015 to 2018. He is currently the Head of the Power Electronics, Machines and Control Research Group, and is the Li Dak Sum Chair Professor in Electrical and Aerospace Engineering with the University of Nottingham, China. He has authored/coauthored 500 academic publications in leading international conferences and journals.

Prof. Wheeler is a member of the IEEE PELs AdCom and was an IEEE PELs Distinguished Lecturer from 2013 to 2017.

Frede Blaabjerg (S'86–M'88–SM'97–F'03) received the Ph.D. degree in electrical engineering from the Aalborg University, Aalborg, Denmark, in 1995.

From 1987 to 1988, he was with the ABB-Scandia, Randers, Denmark. He became an Assistant Professor in 1992, an Associate Professor in 1996, and a Full-Time Professor in power electronics and drives in 1998. In 2017, he became a Villum Investigator. He is honoris causa at the University Politehnica Timisoara, Romania and Tallinn Technical University, Estonia. He has authored/coauthored more than 600 journal papers in the fields of power electronics and its applications. He is the co-author of four monographs and an editor of 10 books in power electronics and its applications. His current research interests include power electronics and its applications, such as in wind turbines, PV systems, reliability, and harmonics and adjustable speed drives.

Prof. Blaabjerg was the Editor-in-Chief of the IEEE TRANSACTIONS ON POWER ELECTRONICS from 2006 to 2012. He has been Distinguished Lecturer for the IEEE POWER ELECTRONICS SOCIETYfrom 2005 to 2007 and for the IEEE INDUSTRY APPLICATIONS SOCIETY from 2010 to 2011 as well as 2017–2018. In 2018, he is President Elect of IEEE POWER ELECTRONICS SOCIETY. He is the Vice-President of the Danish Academy of Technical Sciences. He is nominated in 2014, 2015, 2016, and 2017 by Thomson Reuters to be between the Most 250 Cited Researchers in Engineering in the World. He was the recipient of the 29 IEEE Prize Paper Awards, the IEEE PELS Distinguished Service Award in 2009, the EPE-PEMC Council Award in 2010, the IEEE William E. Newell Power Electronics Award 2014, and the Villum Kann Rasmussen Research Award 2014.